, *Polymer* Vol. 37 No. 13, pp. 2845–2852, 1996

0032-3861/96/$15.00 + 0.00

Structure and phase behaviour of polyazomethines having flexible (*n*-alkyloxy)methyl side chains

Heesub Kim, Sang-Bong Park, Jin Chul Jung and Wang-Cheol Zin*
Department of Materials Science and Engineering, Pohang University of Science and Technology, San 31, Hyoja-dong, Pohang, 790-784, Korea
(Received 18 April 1995)

Structure and phase behaviour of a series of thermotropic polyazomethines having (*n*-alkyloxy)methyl side chains (-CH_2O-*n*-C_mH_{2m+1}, m = 4, 6, 8, 12) have been studied by wide-angle X-ray scattering, differential scanning calorimetry (d.s.c.) and polarizing optical microscopy. In d.s.c. thermograms the samples showed basically three transitions. The first transitions were ascribed to solid–solid transitions resulting from a large increase in disorder of the side chains. The second ones were assigned to crystal–mesophase transitions arising from melting of the side chain crystals. The third ones were attributed to mesophase–isotropic melt transitions. All the samples showed layered structures in the mesophase as well as in the crystalline phase, in which the side chains were fully interdigitated. In the crystalline phase the repeat units of rigid main chain were found not to align parallel with those of neighbouring main chains, but slipped by 49°. In the mesophase the side chain crystals were molten and the layer spacings increased proportionally with increasing side chain length. The structural regularity in the slipped repeat unit disappeared in the polymers bearing long side chains, whereas it was retained in those having short side chains. A unidirectional shearing made the layer plane align parallel on the surface. Copyright © 1996 Elsevier Science Ltd.

(Keywords: rigid rod polymer; polyazomethines; phase behaviour)

INTRODUCTION

In a number of recent publications[1–13] it has been shown that pendent flexible side chains attached to stiff main chains greatly enhance the solubility and fusibility of the rigid-rod polymers and these polymers form a novel layered structure in their crystalline and liquid crystalline phases. The flexible side chains act as a bound solvent or an internal plasticizer for the stiff main chain. The layered structure is characterized by a segregated crystalline structure, in which the main chains form separate layers, with the flexible side chains occupying the space between the main chain layers. The layered mesophase is stabilized by strong attractive interchain interactions exerted by the aromatic main chain[7].

In our previous paper[14] we reported synthesis and properties of polyazomethines having (*n*-alkyloxy)methyl side chains (designated as C_m-PAMs). They were prepared by solution condensation of 2,4-bis((*n*-alkyloxy)methyl)-terephthalaldehydes with *p*-phenylenediamine. In the crystalline phase it was found that they form a layered structure and the side chains emanating from the adjacent backbone layers are tightly interdigitated.

In the present study, we report more detailed structural characteristics of the mesophase as well as the crystalline phase based upon X-ray studies which have been conducted for further elucidation of their structure and phase behaviour.

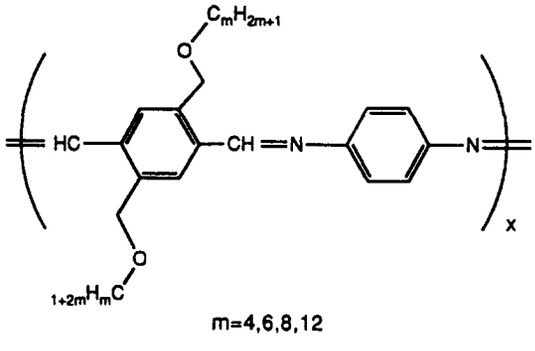

m=4,6,8,12

EXPERIMENTAL

Initial samples for X-ray measurements were powders obtained directly by polymerization. A powder sample of C_{12}-PAM was sheared by unidirectional rubbing in its mesophase, in which only the side chain crystals are molten. Right after shearing it was quenched by immersing into cooled water. It had the form of a film. X-ray reflections ($2° < 2\theta < 35°$) were measured by a Rigaku-Denki X-ray generator in transmission mode using CuKα radiation and a graphite monochromator installed in front of the counter. *In situ* X-ray measurements at varying temperatures were achieved using an electric heating stage. A Kapton window was used to prevent the samples from flowing down after melting and the scattering intensity from the Kapton window was

* To whom correspondence should be addressed

subtracted. X-ray reflections for powder samples at room temperature were measured by a Rigaku-Denki X-ray generator with rotating anode tube in reflection mode. All diffractograms are reported as observed. Differential scanning calorimetry (d.s.c.) measurements were performed on a Perkin Elmer DSC 7 calorimeter at a constant heating rate of 20°C min^{-1}. Polarizing microscopic pictures were taken with a Zeiss MC 100 microscope. Densities were determined by the floating method using aqueous NaCl solutions.

RESULTS AND DISCUSSION

Phase behaviour

In our previous article[14] it was mentioned that the C_m-PAMs show basically three phase transitions in their d.s.c. thermograms, as reproduced in *Figure 1*. The first transitions appearing around 100°C are observable in the C_m-PAMs having longer side chain length than C_4-PAM, and they remain practically unaffected by increasing side chain length. This transition may originate from the solid–solid conversion which corresponds to a large increase in disorder of the side chains, as investigated in a similar system[15]. The C_4-PAM is believed to have such a low volume fraction of side chains that it could not exhibit this solid–solid transition.

The second transitions are observed at varying temperatures. These transitions arise from melting of the crystal phase to form mesophase. They shift drastically to lower temperatures as the side chain length increases. The rapid decrease in melting point results from the increasing volume fraction of side chains acting as bound solvent or internal plasticizer towards the rigid main chains. When C_m-PAM samples existing in the mesophase are placed between two glass plates and pressed, they exhibit fluid-like behaviour, although only a fine grain texture can be obtained from polarizing optical microscopy.

The third transition is observed only in the C_{12}-PAM bearing the longest side chains at ~250°C. This transition occurs from a phase conversion of mesophase to isotropic melt, as confirmed by polarizing optical microscopic investigations. In this sample the volume fraction of its side chains is so high that their action as internal plasticizer towards rigid backbones lowers the third transition down to an observable range, whereas in other samples the volume fraction is not sufficiently high.

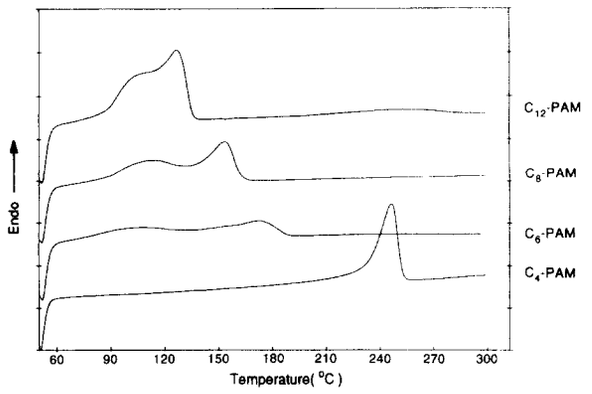

Figure 1 Normalized d.s.c. thermograms of as-polymerized samples of C_m-PAM on heating

All C_m-PAMs, however, show no reproducibility in their d.s.c. measurements but instead show a great thermal hysteresis, since the heat treatment during d.s.c. scans induces further thermal polymerization and thereby increases the molecular weight of the polymers. If the samples reach sufficiently high molecular weight, then the rate of crystallization is lowered to such an extent that practically no crystals can be formed under the usual d.s.c. scan conditions[14,16].

Crystalline structure

Figure 2 displays X-ray diffractograms taken from powder C_m-PAMs at room temperature. In the small-angle region a sharp and strong reflection (designated as A), with its higher orders, as well as a weak one (designated as C) are observable in each C_m-PAM. The A reflections shift to lower angles, as side chain length increases, whereas the C reflections, having an approximate spacing of 9.5 Å ($2\theta = 9.3°$) independent of the side chain length, remain at a constant position. In addition, in the wide-angle region many peaks are observed practically at the same angles, again independent of side chain length.

According to our interpretation of these X-ray data, a layered structure can be proposed for all the C_m-PAMs, as illustrated in *Figure 3*. The crystal lattice is believed to be triclinic, but a precise determination of the whole molecular structure has not been conducted yet and hence we refer to a triclinic lattice only for the main chain structure. In *Table 1* is a summary of the Bragg distances and their respective indices of the main chain structure for two representative samples, C_{12}-PAM and C_6-PAM. The crystal lattice is triclinic with one polymer chain in the unit cell.

As mentioned in the previous paper[14], the 100 reflections (A) arise from the layer spacings between two main chains. The side chains, which are fully interdigitated and tilted with respect to the rigid main

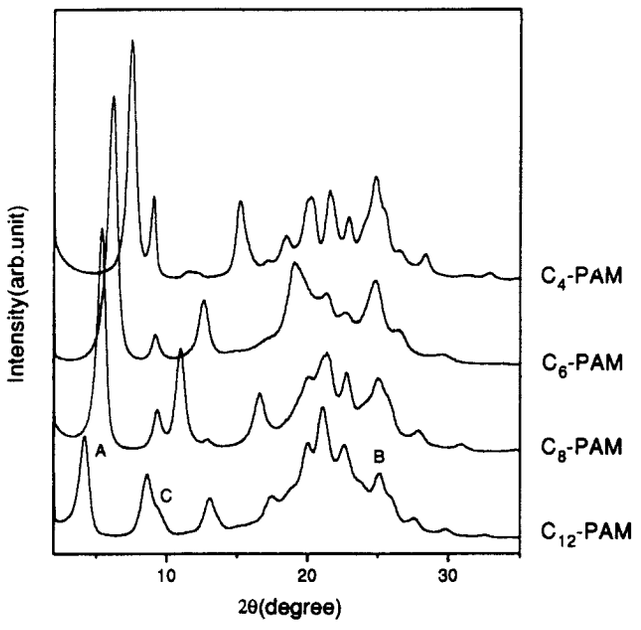

Figure 2 X-ray diffractograms of C_m-PAM taken at room temperature. They were measured from an X-ray generator with rotating anode tube in reflection mode

chain, come to occupy this domain between the main chains. Each layer is formed by a lateral packing of main chains, as can be elucidated from the 010 reflections (B). Weak reflections in the $2\theta = 26–35°$ region can be ascribed to other $h10$ reflections ($h > 0$). As a result, the lateral spacing of the main chain is 3.6 Å, which is close to the van der Waals radius of the phenyl ring (3.45 Å). This suggests that the two phenyl rings of C_m-PAM have nearly coplanar arrangements, while those of benzylidenealine[17], which is very similar in structure to the unsubstituted monomer of C_m-PAM, are known to have no coplanarity.

The length of the repeat unit of the main chain can be calculated from the bond lengths and angles of benzylideneaniline, since benzylideneaniline can be considered as the model compound of the main chain

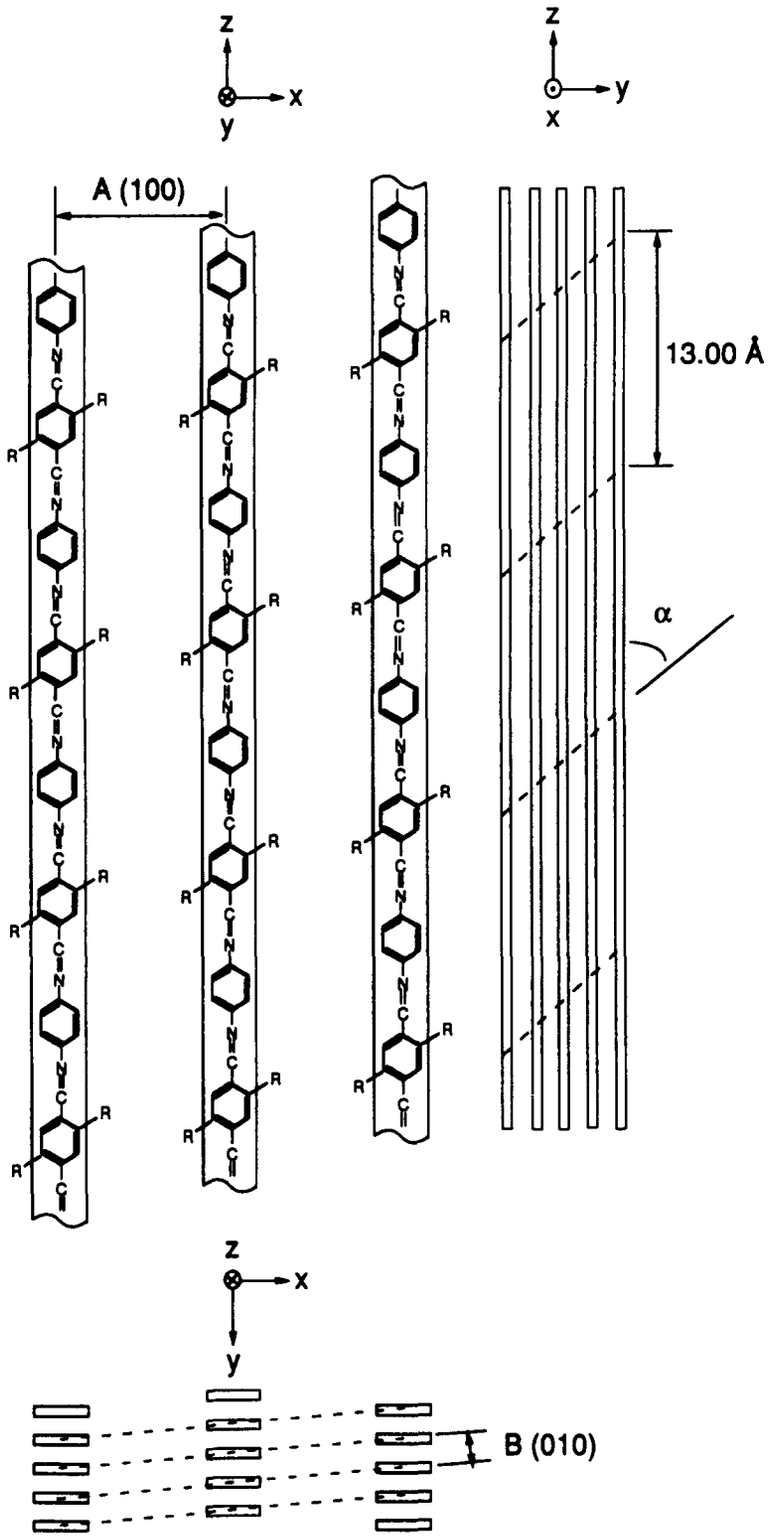

Figure 3 Model of molecular packing of C_m-PAM at the crystalline phase. The main chains are packed into a layer and the side chains are crystallized and occupy the space between the layers

Table 1 Calculated and observed X-ray reflections of main chain structure for C_{12}-PAM and C_6-PAM at room temperature. The crystal lattice is triclinic, with lattice constants of $a = 22.22 \pm 0.09$ Å, $b = 4.73 \pm 0.01$ Å, $c = 13.00 \pm 0.04$ Å, $\alpha = 48.6 \pm 0.1°$, $\beta = 70.5 \pm 0.1°$, $\gamma = 82.5 \pm 0.1°$ for C_{12}-PAM, and $a = 14.61 \pm 0.07$ Å, $b = 4.75 \pm 0.01$ Å, $c = 13.00 \pm 0.04$ Å, $\alpha = 49.6 \pm 0.1°$, $\beta = 76.1 \pm 0.1°$, $\gamma = 87.5 \pm 0.1°$ for C_6-PAM

	C_{12}-PAM		C_6-PAM	
Reflection index (*hkl*)	Calculated spacing (Å)	Observed spacing (Å)	Calculated spacing (Å)	Observed spacing (Å)
100	20.77	20.77	14.02	14.02
010	3.52	3.52	3.58	3.57
001	9.20	9.19	9.51	9.50
011	4.40	4.40	4.45	4.44
110	3.40	3.40	3.35	3.34
210	3.21	3.21	3.01	3.01
310	2.99	3.00		
410	2.75	2.74		

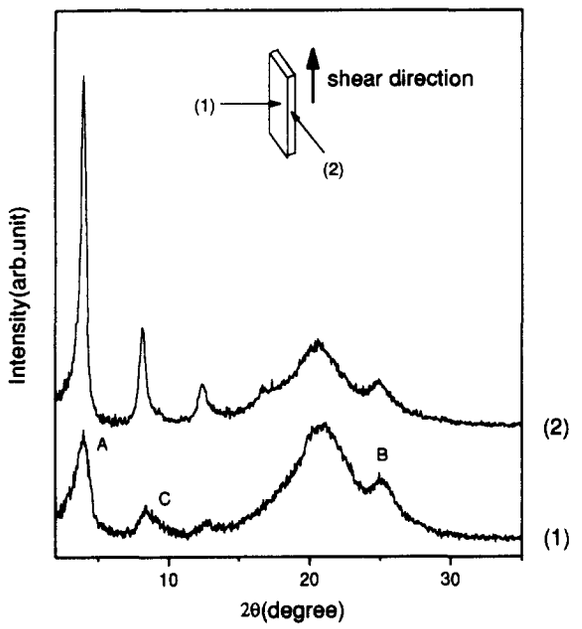

Figure 4 X-ray diffractograms of a sheared sample of C_{12}-PAM taken at room temperature. (1) X-ray beam exposed perpendicular to the film-like surface; (2) X-ray beam exposed parallel to the film-like surface

structure and both are known to have the same anticonfiguration[17,18]. This calculation led to a value of about 13.00 Å, which is consistent with unit cell parameter c (see *Table 1*). As is obvious from unit cell parameter α (see *Table 1*), the repeat units of the rigid main chains are aligned with about 49° of slip, and hence the 001 reflections (C) arise from the slipped structure of the repeat unit. Weak reflections around $2\theta = 20°$ can be attributed to 011 reflections. The fact that phenyl rings on neighbouring backbones are aligned with about 49° of slip results from a steric repulsion between the side chains emanating from the neighbouring backbones. The low intensity of these reflections may be caused by a small electron density difference along the main chain.

To confirm the nature of reflections C, X-ray diffraction for a sheared sample of C_{12}-PAM was carried out at room temperature. *Figure 4* shows the X-ray diffractograms, in which curve 1 is obtained from an X-ray beam exposed perpendicular to the film surface and curve 2 from parallel exposure. For the two diffractograms shown in *Figure 4*, we cannot compare absolute intensities, but only relative ones between curves 1 and 2, because the sample thicknesses for each direction are different. As seen from *Figure 4*, side chains are not crystallized in either curve 1 or 2, because the sample sheared in the mesophase was rapidly quenched. The reflection A related to layer spacing is more intense in 2 than in 1, while the reflections of B, C and the amorphous halo are more intense in 1 than in 2. These results strongly suggest that the shear makes the layer planes align parallel along the shear plane. Therefore, it is evident that the reflections C arise from the slipped structure of the repeat unit.

A lot of wide-angle reflections appearing in the $2\theta = 21$–$24°$ region are not indexed by the above unit cell and can be assigned to the reflections from the ordered alkyloxy side chain crystals that occupy the space between the main chain layers. Analogous reflections are also observed in a number of similar systems[7,8].

To obtain experimental evidence in support of our proposed crystalline structure, we calculated the densities of the C_m-PAMs based on the proposed structure models and compared these density values with the experimentally measured values. The calculation was performed under the assumption that the model structures have 100% crystallinity. As shown in *Figure 5*, the calculated densities have higher values than the measured densities. This results from the fact that the real samples cannot be completely crystalline, but instead have amorphous regions which certainly have lower densities than the crystalline region. Taking this inevitable

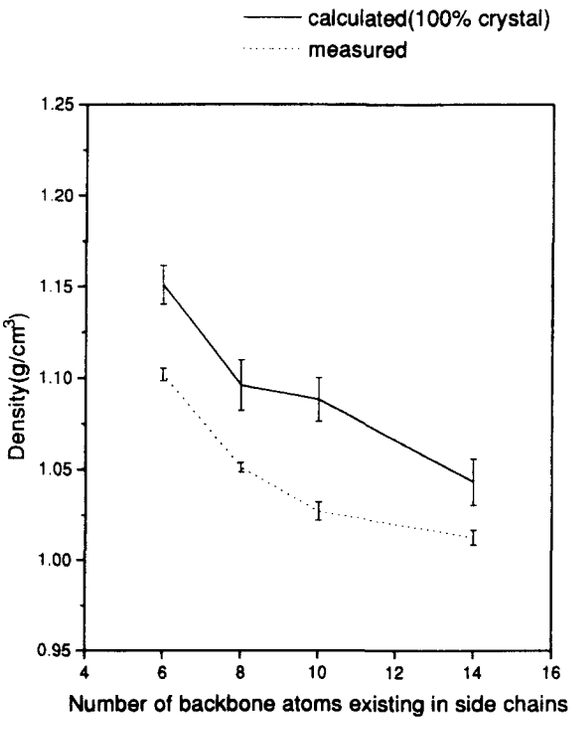

Figure 5 Density comparison of C_m-PAM between experimental values and calculated values at room temperature. The calculated values are based on the unit cells cited in the text

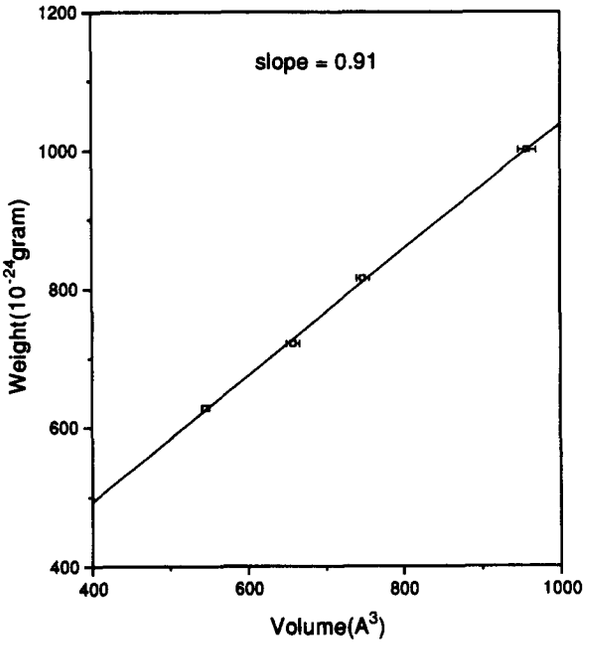

Figure 6 Weight dependence of C_m-PAMs per unit cell volume at room temperature, calculated based on the unit cells as cited in the text

discrepancy into consideration, the calculated density curve is in agreement with the measured density curve, supporting a validity of our structural suggestion.

Figure 5 also shows that density decreases with increasing side chain length. This is quite natural. Since the density of the main chain region is higher than that of the side chain region, the side chain content naturally increases with increasing side chain length, and the whole density must decrease with increasing side chain length.

Figure 6 shows the dependence of the C_m-PAM weight per unit cell volume at room temperature. From the slope of the straight line we can deduce the density of the side chain domain: it is 0.91 g cm^{-3}, which is much higher than that of amorphous *n*-alkanes of the same chain length (0.659–0.763 g cm^{-3} at 20°C). This provides additional evidence that the side chains are crystalline at room temperature.

Mesophase structure

To investigate structural changes taking place at the transitions shown in the d.s.c. thermograms (*Figure 1*), X-ray diffractograms for powders were measured at temperatures corresponding to the different phase regions. *Figure 7* shows X-ray diffractograms of C_{12}-PAM taken at different temperatures. Immediately after passing the solid–solid transitions (110°C), there is no significant change in the X-ray diffractograms. Only side chain reflections change to somewhat broad and diffuse peaks. After passing the crystal–mesophase transition (140°C), there are drastic changes in the X-ray diffractograms. The reflection A, corresponding to the layer spacing, suddenly shifts to a smaller angle and its intensity suddenly increases. In addition, the intensity of its higher order peaks decreases. The reflection C, corresponding to the slipped repeat unit, disappears. Many wide-angle reflections, except a reflection B arising from lateral backbone spacing, disappear and form a broad halo typical for a liquid. Disappearance of the *h*10 reflections ($h > 0$) reveals that in the mesophase the

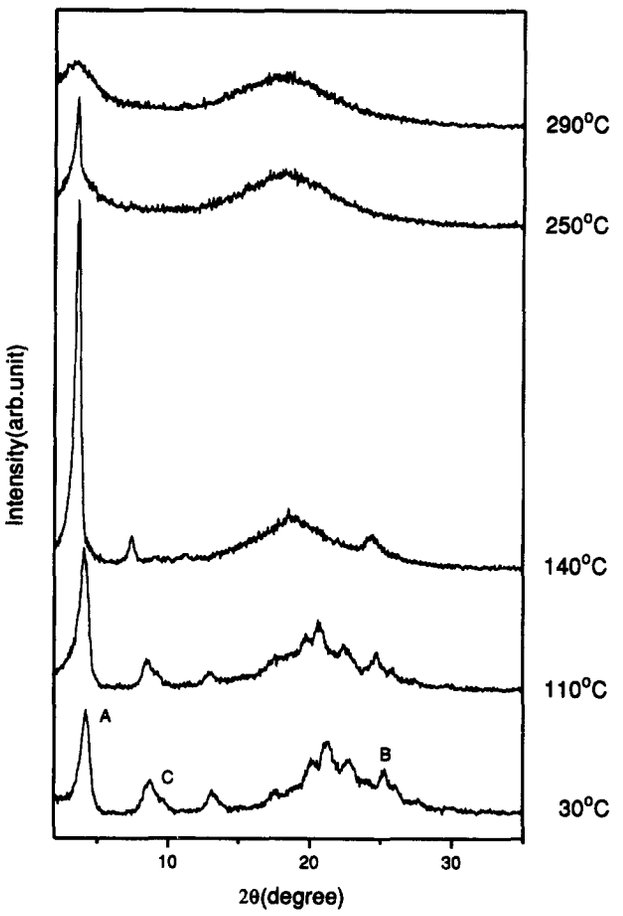

Figure 7 X-ray diffractograms of C_{12}-PAM taken at different temperatures

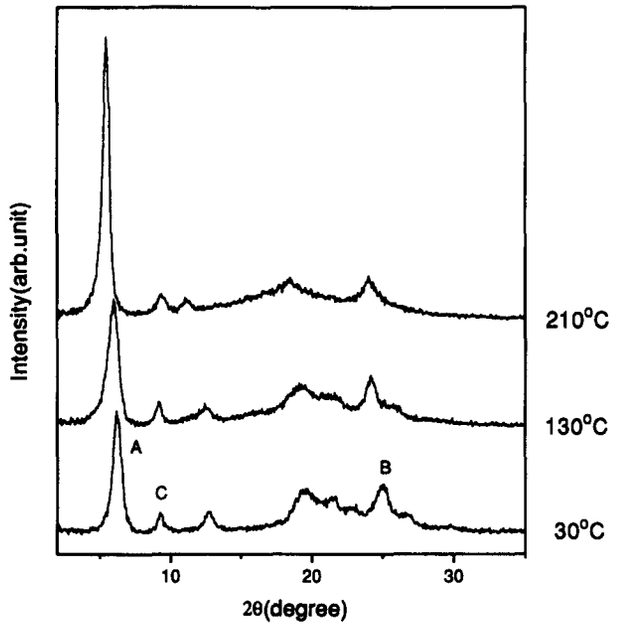

Figure 8 X-ray diffractograms of C_6-PAM taken at different temperatures

correlation between adjacent backbone layers has been disrupted. After passing the mesophase–isotropic transition (290°C), the reflections B and A disappear completely. As is obvious from the X-ray diffractogram

Table 2 Observed X-ray reflections for C_{12}-PAM at 140°C and C_6-PAM at 210°C

Reflection index (*hkl*)	C_{12}-PAM (Å)	C_6-PAM (Å)
100	24.19	16.06
010	3.64	3.69
001	–	9.35
011	–	4.83

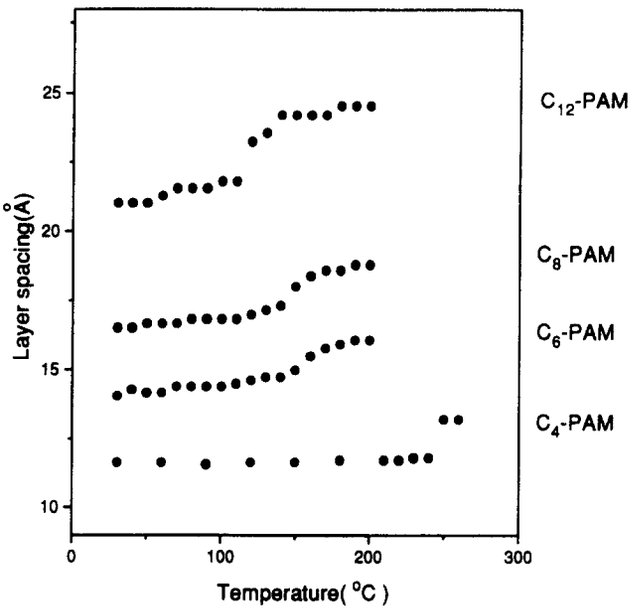

Figure 9 Temperature dependence of the layer spacing of C_m-PAMs. The layer spacings were measured by wide-angle X-ray scattering (WAXS)

at 250°C, the reflection B disappears earlier than the reflection A during this transition. This fact suggests that incompatibility between aromatic backbones and aliphatic side chains is stronger than the attractive interchain interaction between aromatic backbones.

Figure 8 shows X-ray diffractograms of C_6-PAM taken at different temperatures. Since C_4- and C_8-PAMs showed similar features to C_6-PAM, only the X-ray diffractogram of the latter is reproduced as a representative example. At the solid–solid transition, C_6-PAM reveals similar X-ray diffraction features to C_{12}-PAM. At the crystal–mesophase transition, however, the C and 011 reflections do not disappear and the C reflection shifts slightly to a wider angle. This behaviour is related to a structural change accompanied by melting of the side chain crystals. Melting of the side chain crystal accompanies a change of the positional order in each layer. The structural regularity in the slipped repeat unit disappears in C_{12}-PAM, whereas it does not in C_6-PAM. In C_6-PAM the slip angle was calculated from the 001 reflection to be 46.0°. This value is not substantially different from the slip angle of 49.6° measured for the C_6-PAM crystal at room temperature. Therefore, in the mesophase the structural regularity in the slipped repeat unit is maintained in C_6-PAM and hence also in C_4-PAM and C_8-PAM, while it is disrupted in C_{12}-PAM. In *Table 2* is a summary of the Bragg distances and their respective indices for both C_6-PAM and C_{12}-PAM in the mesophase.

The drastic changes in X-ray diffractograms after crystal–mesophase transition can be explained as follows. After the transition the side chain crystal melts, but the layered structure with regular lateral spacing of backbones is maintained due to strong incompatibility between aromatic main chains and aliphatic side chains and strong attractive interaction between aromatic backbones. The side chain melting results in an increase of the volume of the side chain region and hence an increase of layer spacing. The intensity of the reflection from the layer spacing jumps suddenly, since the side chain melting results in a sudden jump in electron density difference between the molten side chain and the still unmolten backbone domain. The fact that only the first and the second order of A reflections are sustained indicates that the layered structure that is not destroyed in the mesophase is not so highly ordered as at 30°C.

To observe the effect of side chain melting on structural change by X-ray diffractometry, the temperature dependence of layer spacing was measured, as shown in *Figure 9*. At temperatures lower than the crystal–mesophase transition, there is no substantial change on layer spacing except a small increase resulting from thermal expansion. After the transition the layer spacing jumps suddenly and the increment is proportional to the side chain length. This behaviour is certainly ascribable to a sudden volume increase resulting from the melting of the side chain crystal. Once mesophase is formed, the layer spacing does not bring any substantial change except a small increase due to thermal expansion. This demonstrates clearly that the rigid backbones are still regularly aligned in mesophase.

Figure 10 shows layer spacings as a function of the number of backbone atoms existing in side chains, as measured in the mesophase. The observed layer spacing values plot with good linearity except that of C_4-PAM determined at 200°C. The exceptional discrepancy of C_4-

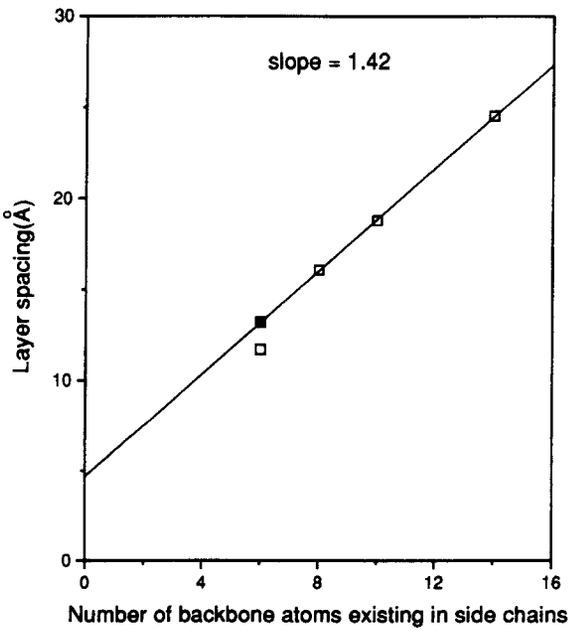

Figure 10 Layer spacings of C_m-PAMs as a function of the number of backbone atoms existing in side chains, as measured in the mesophase; □, 200°C; ■, 260°C

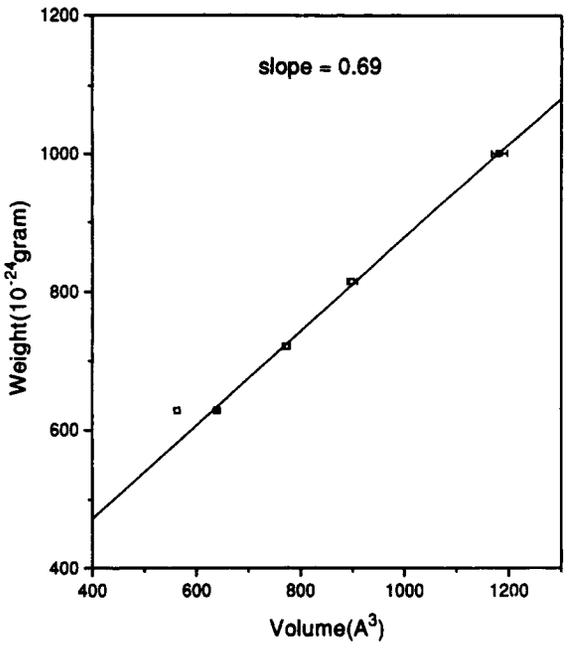

Figure 11 Weight dependence of C_m-PAMs per unit volume in the mesophase. It was calculated based on the unit volume which is equal to (layer spacing) × (lateral spacing of main chains) × (length of repeat unit) and contains one polymer chain: □, 200°C; ■, 260°C

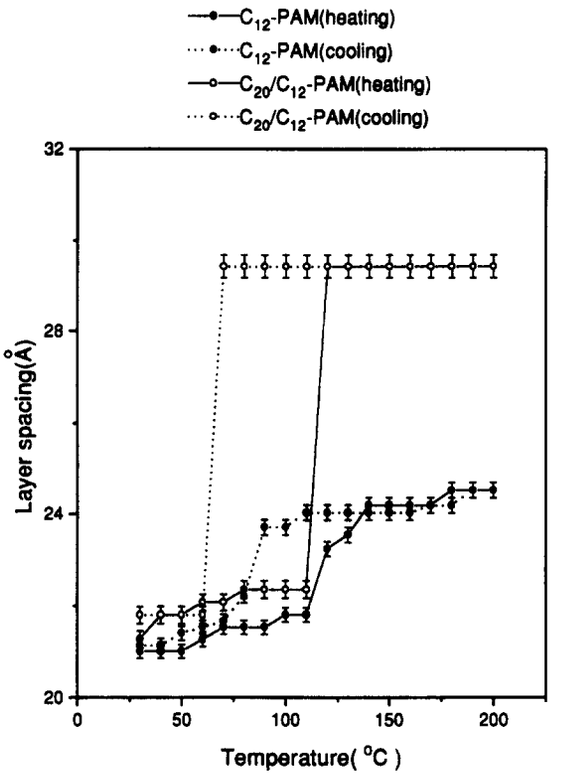

Figure 12 Temperature dependence of the layer spacing of C_{12}-PAM and C_{20}/C_{12}-PAM blend. The layer spacings were measured by WAXS

PAM results from the fact that the melting point of the side chain crystal is 247°C, and hence at 200°C no sudden increase in volume of the side chains has yet taken place. In C_6-, C_8- and C_{12}-PAMs the side chain crystals are completely molten at 200°C, since their crystal–mesophase transition temperatures lie at 172, 154 and 127°C, respectively. The intercept value 4.7 Å can be ascribed to the width of the rigid backbone,

In *Figure 10* the slope of the linear line is determined to be 1.42 Å per CH_2 group. This value corresponds to an increment of side chain length per CH_2 group. This value is much larger than the value of 1.25 Å per CH_2 unit which is effective for the crystalline structure of the side chains emanating perpendicularly from the PAM backbones. The large difference between these two increment values indicates that in the mesophase the side chains are molten.

Figure 11 shows the weight dependence of C_m-PAMs per unit volume measured in the mesophase. Again, it shows a good linearity except for C_4-PAM determined at 200°C. From the slope of the line we can deduce the density of the side chain region in the mesophase. This density was determined to be 0.69 g cm^{-3}, which is much lower than that of the crystalline phase (0.91 g cm^{-3}). This large difference in density also confirms that the side chain domains are molten and amorphous in the mesophase state.

In the mesophase side chains are molten and occupy the space between backbone layers, then chemically analogous *n*-alkanes may be miscible with the molten side chains and may penetrate into the side chain region. To study that, an equal weight of C_{20} eicosane (m.p. 36–38°C) was added to the C_{12}-PAM and the layer spacings for the blends were determined at various temperatures. *Figure 12* shows the temperature dependences for C_{12}-PAM itself as well as the C_{20}/C_{12}-PAM blend. From the lower heating curve for C_{12}-PAM it is seen that the layer spacing jumps suddenly at about 120°C. This jump point corresponds to the crystal–mesophase transition temperature measured by d.s.c. (*Figure 1*). This result shows that a phase transition temperature has also been determined by wide-angle X-ray scattering. From the upper heating curve for the C_{20}/C_{12}-PAM blend we can also see the presence of a sudden jump at about 120°C. The fact that both the lower and the upper heating curves have a jump at the same temperature indicates that no attractive interaction exists between the side chain crystal and the molten eicosane. Immediately after the side chain crystals melt and become amorphous, then C_{20} can penetrate, driven by the miscibility. The jump naturally results in a remarkable increase in the volume of the side chain domain. The higher jump observed in the C_{20}/C_{12}-PAM blend than in pure C_{12}-PAM results from an increase in side chain domain, because the eicosane molecules which are miscible with molten side chain molecules have penetrated into this amorphous region.

ACKNOWLEDGEMENT

This work was supported by the Korea Science and Engineering Foundation (92-48-00-01).

REFERENCES

1 Ballauff, M. *Makromol. Chem. Rapid Commun.* 1986, **7**, 407
2 Ballauff, M. *Macromolecules* 1986, **19**, 1366
3 Ballauff, M. and Schmidt, G. F. *Makromol. Chem. Rapid Commun.* 1987, **8**, 93
4 Ballauff, M. and Schmidt, G. F. *Mol. Cryst. Liq. Cryst.* 1987, **147**, 163
5 Berger, K. and Ballauff, M. *Mol. Cryst. Liq. Cryst.* 1988, **157**, 109

6 Ballauff, M., Rosenau-Eichin, R. and Fischer, E. W. *Mol. Cryst. Liq. Cryst.* 1988, **155**, 211
7 Rodriguez-Parada, J. M., Duran, R. and Wegner, G. *Macromolecules* 1989, **22**, 2507
8 Ballauff, M. *Angew, Chem., Int. Edn Engl.* 1989, **28**, 253
9 Harkness, B. R. and Watanabe, J. *Macromolecules* 1991, **24**, 6759
10 Stern, R., Ballauff, M., Leiser, G. and Wegner, G. *Polymer* 1991, **32**, 11
11 Galda, P., Kistner, D., Martin, A. and Ballauff, M. *Macromolecules* 1993, **26**, 1595
12 Watanabe, J., Harkness, B. R., Sone, M. and Ichimura, H. *Macromolecules* 1994, **27**, 507
13 Kriecheldorf, H. R. and Domschke, A. *Macromolecules* 1994, **27**, 1509
14 Park, S.-B., Kim, H., Zin, W.-C. and Jung, J. C. *Macromolecules* 1993, **26**, 1627
15 Whittaker, A. K., Falk, U. and Spiess, H. W. *Makromol. Chem.* 1989, **190**, 1603
16 Suematsu, K., Nakamura, K. and Takeda, J. *Polym. J.* 1983, **15**, 71
17 Burgi, H. B. and Dunitz, J. D. *Helv. Chem. Acta* 1970, **53**, Fasc. 7, 206
18 Natansohn, A., Yang, H. and Clark, C. *Macromolecules* 1991, **24**, 5489